Micro-bubbles and Micro-particles are Not Faithful Tracers of Turbulent Acceleration

Varghese Mathai,[1] Enrico Calzavarini,[2,*] Jon Brons,[1,3] Chao Sun,[4,1,†] and Detlef Lohse[1,5]

[1] *Physics of Fluids Group, Faculty of Science and Technology, Mesa+ Institute, University of Twente, 7500 AE Enschede, The Netherlands.*
[2] *Univ. Lille, CNRS, FRE 3723, LML, Laboratoire de Mecanique de Lille, F 59000 Lille, France*
[3] *Department of Mathematics and Physics, Faculty of Engineering and Computing, Coventry University, United Kingdom*
[4] *Center for Combustion Energy and Department of Thermal Engineering, Tsinghua University, 100084 Beijing, China.*
[5] *Max Planck Institute for Dynamics and Self-Organization, 37077 Göttingen, Germany.*

(Dated: August 22, 2016)

We report on the Lagrangian statistics of acceleration of small (sub-Kolmogorov) bubbles and tracer particles with Stokes number St $\ll$1 in turbulent flow. At decreasing Reynolds number, the bubble accelerations show deviations from that of tracer particles, i.e. they deviate from the Heisenberg-Yaglom prediction and show a quicker decorrelation despite their small size and minute St. Using direct numerical simulations, we show that these effects arise due the drift of these particles through the turbulent flow. We theoretically predict this gravity-driven effect for developed isotropic turbulence, with the ratio of Stokes to Froude number or equivalently the particle drift-velocity governing the enhancement of acceleration variance and the reductions in correlation time and intermittency. Our predictions are in good agreement with experimental and numerical results. The present findings are relevant to a range of scenarios encompassing tiny bubbles and droplets that drift through the turbulent oceans and the atmosphere. They also question the common usage of micro-bubbles and micro-droplets as tracers in turbulence research.

arXiv:1606.02050v1 [physics.flu-dyn] 7 Jun 2016

Heavy and light particles caught up in turbulent flows often behave differently from fluid tracers. The reason for this is usually the particle's inertia, which can drive them along trajectories that differ from those of the surrounding fluid elements [1–4]. Due to their inertia, measured by the Stokes number St[1], such particles depart from fluid streamlines and distribute nonhomogeneously even when the carrier flow is statistically homogeneous [3, 5–11]). Numerical studies have captured several interesting effects of particle inertia through point-particle simulations in homogeneous isotropic turbulence [7, 12–14]. For instance, with increasing inertia, light particles showed an initial increase in acceleration variance (up to a value $\langle a^2 \rangle \sim 9$ times the tracer value) followed by a decrease, while heavy particles showed a monotonic trend of decreasing acceleration variance [15]. Such modifications of acceleration statistics arose primarily from the slow temporal response of these inertial particles, i.e when St was finite [9, 16–19]. In comparison, a lower limit of inertia can be imagined (St $\ll 1$), when the particles respond to even the quickest flow fluctuations and, hence, are often deemed good trackers of the turbulent flow regardless of their density ratio [3, 15, 16, 20]. The widespread use of small bubbles and droplets in flow visualization and particle tracking setups (e.g. Hydrogen bubble visualization and droplet-smoke-generators) is founded on this one assumption − that St $\ll 1$ renders a particle responsive to the fastest fluctuations of the flow [21–25].

In many practical situations, particles are subjected to body forces, typically gravitational or centrifugal [26]. This can be the case for rain droplets and aerosols settling through clouds, and tiny air bubbles and plankton drifting through the oceans [27, 28]. The effects of gravitational settling were first brought to light through numerical studies using random and cellular flow fields [29–33]. Their findings were instrumental in highlighting the role of gravity on the clustering and the enhancement of settling velocities of heavy particles in a flow. More recently, inertial effects on settling particles were analysed using direct numerical simulations of fully developed homogeneous isotropic turbulence [17, 18, 34–36]. These revealed that gravity can lead to major modifications of particle clustering, relative velocity and pair statistics, which could be characterized as a function of St and the ratio of turbulent to gravitational acceleration: a_η/g.

While the effects of gravity on particle settling velocity and clustering were shown to be significant [33, 34], another crucial observable of Lagrangian turbulence is the particle's acceleration statistics (variance, correlation and intermittency). Acceleration is important because its variance and time correlation are tightly linked to the energy dissipation rate, a quantity central to characterizing turbulent flows. Yet another feature unique to turbulent flows is the high level of intermittency, or deviations from Gaussian statistics. Acceleration flatness is key to quantifying this for turbulent flows. Therefore, a generic description of these quantities for rising and settling particles of arbitrary density is desirable.

In this Letter, we present the Lagrangian acceleration statistics of small air-bubbles and neutrally buoyant tracer particles in a turbulent water flow where the Taylor-Reynolds number Re_λ is varied in the range $130 - 300$. At decreasing Re_λ the bubble accelerations

[1] Stokes number, St $\equiv \tau_p/\tau_\eta$, where τ_p is the particle response time, and τ_η is the Kolmogorov time scale of the flow.

show deviations compared to tracer particles, which occur despite their very small St (0.004 – 0.017) and small particle size. To explain these, we conduct DNS of particles in homogeneous isotropic turbulence, which reveals that the deviations arise due to the drift of these particles through the turbulent flow. We develop a generic theory that predicts these gravity-induced deviations for an arbitrary density particle, with the ratio St/Fr or equivalently the ratio of particle drift velocity to Kolmogorov velocity, as the relevant parameter controlling the deviations from ideal tracer behavior. Further, we provide insight into the modification of intermittency of particle acceleration arising due to gravity.

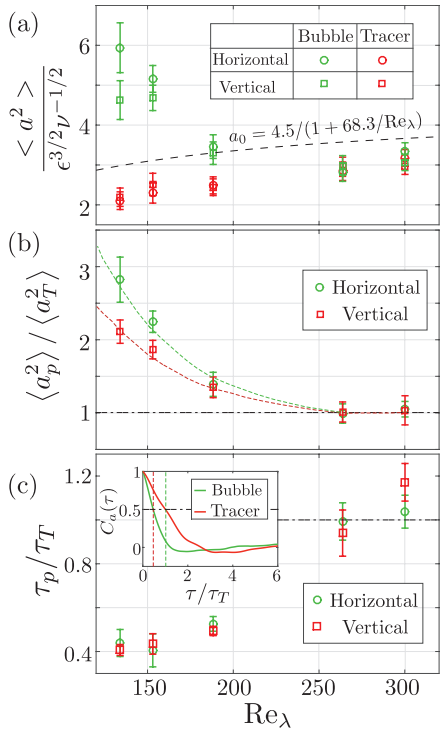

FIG. 1: (a) Heisenberg-Yaglom constant, a_0, estimated for bubbles and tracer particles from experiments at different Re_λ. The dashed curve gives the a_0 estimate according to [37]. (b) Normalized acceleration variance and (c) correlation time of acceleration for bubbles vs Re_λ from experiments. $\langle a_T^2 \rangle$ is the tracer particle acceleration variance. τ_p and τ_T are defined as the 0.5 crossing time of correlation for bubbles and tracer particles, respectively. Inset: Normalized correlation function of acceleration, $C_a(\tau)$, at the lowest $\mathrm{Re}_\lambda \approx 134$.

The experiments were performed in the Twente Water Tunnel facility (TWT), in which an active grid generated nearly homogeneous and isotropic turbulence in the measurement section [38]. The turbulent flow was characterized using hot-film anemometry technique at different Re_λ (see Table I). Small bubbles ($\approx 150 \pm 25$ μm) were generated by blowing pressurized air through a porous ceramic plate. The particles were imaged using a high-speed camera (Photron PCI-1024) at a recording rate

TABLE I: Flow characteristics in the Twente Water Tunnel. Re_λ – the Taylor-Reynolds number (approximate), St – the bubble Stokes number, and a_η/g the ratio of turbulent to gravitational acceleration [34].

Re_λ	134	153	188	263	301
St	0.004	0.005	0.008	0.011	0.017
a_η/g	0.0016	0.0026	0.0044	0.0072	0.0141
St/Fr	4.899	4.159	3.498	2.953	2.363

of 1000 fps. The camera moved on a traverse system, and illumination was provided using a 100 W Pulsed Laser (Litron LDY-303HE) (see Fig. 1 in supplemental material [39]). Similar moving camera setups have been used with heavy particles in a wind tunnel [40], however, the tracking duration was short in those experiments. In the present case, we introduce a novel experimental modification, which allows for long particle trajectories to be recorded. We placed a mirror inside the tunnel at 45° inclination with the horizontal (see Fig. 1 in supplemental material [39]). The laser beam was expanded into a volume, which was reflected vertically by the mirror. Obtaining the acceleration from position data requires accurate determination of higher derivatives. We have here combined the conventional Gaussian-kernel smoothening method with a smoothing-spline based technique [41, 42] which eliminated biases due to a priori choice of filter windows and ensured reliable estimates of the acceleration.

We first address the question of how the bubble accelerations compare to that of similar-sized neutrally buoyant particles at different Re_λ. According to the prediction by Heisenberg and Yaglom [43], the single-component variance of acceleration should follow the relation $\langle a^2 \rangle = a_0 \epsilon^{3/2} \nu^{-1/2}$, where ϵ is the dissipation rate, and ν the kinematic viscosity. In Fig 1(a), we plot the Heisenberg-Yaglom constant a_0 for bubbles along with that for tracer particles. At high Re_λ, the bubbles behave similarly to tracers, with comparable a_0. However, at low Re_λ the bubbles show deviations from tracers, with an elevated a_0. The horizontal acceleration shows the greatest deviation, with $a_0 \approx 6$, while for the vertical component, $a_0 \approx 4.5$ at $\mathrm{Re}_\lambda \approx 134$. For neutrally buoyant tracer particles, a_0 is lower, ≈ 2.1 at $\mathrm{Re}_\lambda \approx 134$, and shows a marginal increase with Re_λ. Thus, the horizontal component of the acceleration variance for bubbles is almost three times that of the tracer value at the lowest Re_λ (see Fig. 1(b)). This is also reflected in the correlation time for bubbles (Fig. 1(c) & Inset), which is shorter compared to that of tracers. These deviations are surprising, since the lowest Re_λ corresponds also to the smallest St in our experiments (see Table. I).

From Fig 1(b), we also note that the vertical component of acceleration is consistently lower as compared to the horizontal one. This anisotropy is not inherent

in the carrier flow [44] and therefore suggests the role of gravity [30]. We note that with decreasing Re_λ, the ratio of turbulent to gravitational acceleration, a_η/g, decreases in our experiments (Table. I). In order to investigate this effect in a systematic way, we perform DNS of homogeneous isotropic turbulence at $\mathrm{Re}_\lambda \approx 80$ in the presence of gravity. For the particles, we use a model considering a dilute suspension of passively advected point-spheres acted upon by inertial and viscous (Stokes drag) forces (see supplemental material [39]). We neglect lift, history and finite-size Faxén forces, since these are verified to be negligible in the point particle limit [15, 45]. The model equation of motion for a small inertial particle advected by a fluid flow field, $(\mathbf{U}(\mathbf{X}(\mathcal{T}),\mathcal{T}))$, may be written as:

$$\ddot{\mathbf{X}} = \frac{3\rho_f}{\rho_f + 2\rho_p}\left(\frac{D\mathbf{U}}{D\mathcal{T}} + \frac{12\nu}{d_p^2}(\mathbf{U}-\dot{\mathbf{X}}) + g\,\hat{\mathbf{e}}_z\right) - g\,\hat{\mathbf{e}}_z, \tag{1}$$

where ρ_f and ρ_p are the fluid and particle mass densities, respectively, d_p is the particle diameter, and $\hat{\mathbf{e}}_z$ is the unit vector in the direction of gravity. The particles under consideration are buoyant ($0 \le \Gamma < 1$) and have very small Stokes number ($\mathrm{St} \approx 0.05$). We vary the gravity intensity g for these particles, resulting in a range of values for a_η/g, according to the Froude number definition in [18, 34]. We first address the case of bubbles ($\Gamma = 0$ in Fig. 2) at various strengths of g. With increasing g, we recover the trends observed in our experiments, i.e. the bubble acceleration variance increases. Gravity enhances the acceleration in both vertical and horizontal directions, and this is accompanied by a decrease in correlation time (see supplemental material [39]).

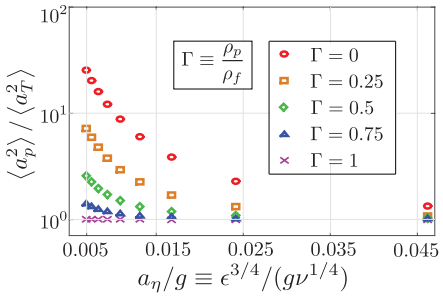

FIG. 2: Normalized horizontal acceleration variance for buoyant particles vs a_η/g obtained from Eulerian-Lagrangian DNS at $\mathrm{Re}_\lambda \approx 80$.

Fig. 2 clearly demonstrates the role of gravity in enhancing the particle's acceleration variance. At the same time, we note that the degree of enhancement diminishes with growing Γ even at fixed a_η/g. Also, the effect of gravity on $\langle a_p^2\rangle/\langle a_T^2\rangle$ appears more pronounced in our simulations (see Fig. 1(b)) and Table I). Thus, the Froude number, if defined as a_η/g [18, 34], can only give a qualitative prediction of the gravity effect. An exact prediction for an arbitrary-density particle is missing.

For a better appreciation of the contribution of gravity to the particle dynamics, we non-dimensionalize eq. (1) in terms of the Kolmogorov length η and time scales τ_η. We obtain

$$\ddot{\mathbf{x}} = \beta\frac{D\mathbf{u}}{Dt} + \frac{1}{\mathrm{St}}(\mathbf{u}-\dot{\mathbf{x}}) + \frac{1}{\mathrm{Fr}}\hat{\mathbf{e}}_z, \tag{2}$$

where $\mathrm{St} \equiv d_p^2/(12\beta\nu\tau_\eta)$ is the Stokes number and $\mathrm{Fr} \equiv a_\eta/((\beta-1)g)$ is a buoyancy-corrected Froude number that takes the particle density, through $\beta \equiv 3\rho_f/(\rho_f + 2\,\rho_p)$, into account. In this situation, two important small-Stokes limits may be considered [17, 30]. At high turbulence intensities ($\mathrm{Fr} \to \infty$), the third term on the right-hand-side of eq. (2) may be neglected. This leads to the well known result $\ddot{\mathbf{x}} \simeq D_t\mathbf{u}$ for particle acceleration, where $D_t\mathbf{u}$ is the fluid tracer acceleration. However, for small Fr, the small St limit leads to the result $\ddot{\mathbf{x}} = D_t\mathbf{u} + \frac{\mathrm{St}}{\mathrm{Fr}}\partial_z\mathbf{u}$ for particle acceleration. By employing results from homogeneous isotropic turbulence (see supplemental material [39]), one obtains the following relations linking the acceleration variance of particles to that of the fluid tracer:

$$\frac{\langle a_h^2\rangle}{\langle a_T^2\rangle} \equiv \frac{\langle \ddot{x}^2\rangle}{\langle (D_t u_x)^2\rangle} \simeq 1 + \frac{2}{15a_0}\left(\frac{\mathrm{St}}{\mathrm{Fr}}\right)^2, \tag{3}$$

$$\frac{\langle a_v^2\rangle}{\langle a_T^2\rangle} \equiv \frac{\langle \ddot{z}^2\rangle}{\langle (D_t u_x)^2\rangle} \simeq 1 + \frac{1}{15a_0}\left(\frac{\mathrm{St}}{\mathrm{Fr}}\right)^2, \tag{4}$$

where a_h and a_v are the horizontal and vertical accelerations, respectively, for an arbitrary-density particle, a_T is the tracer particle acceleration, and x and z represent the horizontal and vertical directions, respectively.

In Fig. 3, we compare the normalized acceleration variance vs St/Fr from experiment with our theoretical predictions (eq. (3) & (4)). The dashed lines show the theoretical predictions using the a_0 from the present experiments (Fig. 1(a)). The experimental data-points are in reasonable agreement with our predictions. Therefore, the apparent Re_λ dependence that was seen in our water tunnel experiments (Fig. 1) is in fact a St/Fr effect, since the St/Fr increases with decreasing Re_λ in our experiments (see Table I).

The present bubble-tracking experiments cover a narrow range of $\mathrm{St/Fr} = [2-5]$ at fixed density-ratio ($\beta = 2.99$), while eq. (3) & (4) should be valid for arbitrary density-ratio. To test this, we compare the results of DNS for an extended range of density-ratios $\beta = [0, 3]$ and $\mathrm{St/Fr} = [-10, 20]$. In Fig. 4(a), the left half ($\mathrm{St/Fr} < 0$) points to heavy particles, and the right one ($\mathrm{St/Fr} > 0$), to buoyant particles. The predicted quadratic dependence on St/Fr and even the pre-factors $2/(15a_0)$ and $1/(15a_0)$ for the horizontal and vertical components, respectively, are in agreement with our simulations. We note that for sufficiently large Reynolds numbers, a_0 is practically constant [43], and the ratio St/Fr becomes

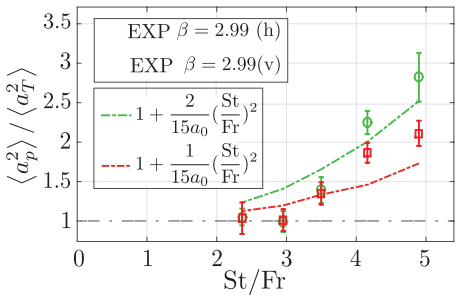

FIG. 3: Normalized acceleration variance in horizontal (h) and vertical (v) directions vs St/Fr for bubbles from our experiments. The dashed lines give the predictions based on the eq. (3) & (4), using a_0 obtained for the tracer particles in the present experiments (Fig. 1(a)).

the sole control parameter governing the enhancement of acceleration variance. Therefore, our results have broad applicability, to even large Re_λ atmospheric and oceanic flows. In Fig. 4(b), we present the numerical results for the tracer-normalized correlation time in the presence of gravity. We propose a model for the correlation time based on the time a particle takes to cross an energetic eddy of the flow (see supplemental material [39]). The model predicts a behavior of the form $\tau_p/\tau_T \approx \frac{1}{1+\mathrm{k}\ (\mathrm{St}/\mathrm{Fr})}$, where $\mathrm{k} \approx \sqrt[4]{\frac{5}{3\mathrm{Re}_\lambda^2}}$. The numerical results are in reasonable agreement with our predictions. Small deviations are noticeable in the small St/Fr range. In this range, the fluid acceleration $D_t\mathbf{u}$ dominates over the the velocity gradient $\frac{\mathrm{St}}{\mathrm{Fr}}\partial_z\mathbf{u}$. This explains the slower decline than what is predicted by our model in the small St/Fr range (see supplemental material [39]). We also notice that the horizontal component (hollow symbols) is slightly higher that the vertical one (solid symbols) in the small St/Fr range. This is because the transverse velocity gradients $\partial_z u_x$ are longer correlated than the longitudinal velocity gradients $\partial_z u_z$ (see supplemental material [39]).

While the effects of gravity on acceleration variance and correlation time have been comprehensively demonstrated, its role on the intermittency of particle acceleration is not clear. Intermittency, i.e. the observed strong deviations from Gaussianity, can be characterized in terms of the flatness of acceleration $\mathcal{F}(a_p) \equiv \langle a_p^4 \rangle / \langle a_p^2 \rangle^2$. Assuming statistical independence between $D_t u_i$ and $\partial_z u_i$, we obtain the tracer-normalized flatness of the particle acceleration, $\mathcal{F}(a_p)/\mathcal{F}(a_T)$, as a decreasing function of St/Fr (see supplemental material [39]). At large St/Fr, we asymptotically approach the limits

$$\frac{\mathcal{F}(a_h)}{\mathcal{F}(a_T)} \equiv \frac{\mathcal{F}(\ddot{x})}{\mathcal{F}(D_t u_x)} \simeq \frac{\mathcal{F}(\partial_z u_x)}{\mathcal{F}(D_t u_x)}, \tag{5}$$

$$\frac{\mathcal{F}(a_v)}{\mathcal{F}(a_T)} \equiv \frac{\mathcal{F}(\ddot{z})}{\mathcal{F}(D_t u_x)} \simeq \frac{\mathcal{F}(\partial_z u_z)}{\mathcal{F}(D_t u_x)}, \tag{6}$$

It is verified that $\mathcal{F}(\partial_z u_z) < \mathcal{F}(\partial_z u_x) < \mathcal{F}(D_t u_x)$ [46].

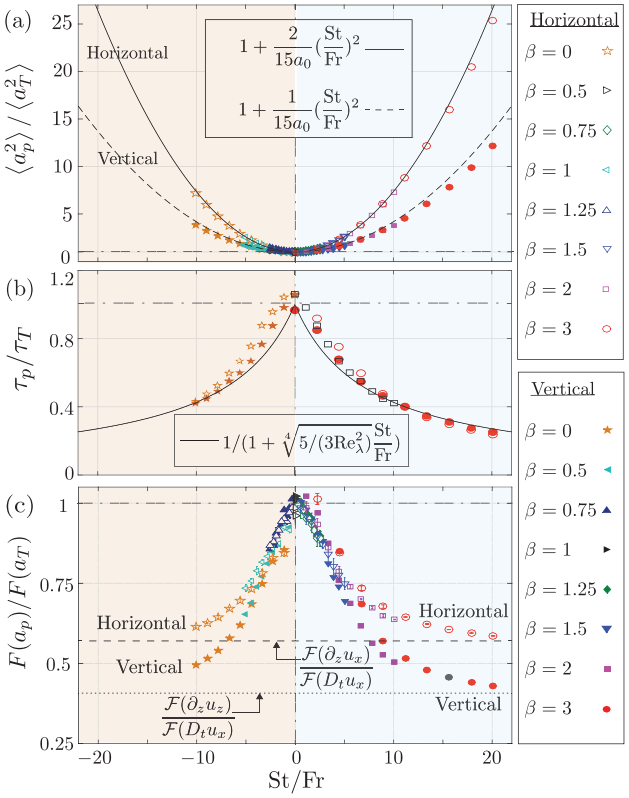

FIG. 4: (a) Normalized acceleration variance, (b) normalized correlation time, and (c) normalized flatness factor vs St/Fr for a family of buoyant and heavy particles, obtained from DNS. Solid and dashed curves in (a) show our theory-predictions for horizontal and vertical accelerations, respectively (eq. (3) & (4)). (b) The black curve shows the theoretical prediction for correlation-time. (a)-(c) Hollow and solid symbols correspond to horizontal and vertical components, respectively.

This leads to the prediction $\mathcal{F}(a_v) < \mathcal{F}(a_h)$, i.e. vertical acceleration is less intermittent as compared to the horizontal one. In Fig. 4(c), we present the normalized flatness factor from our simulations for an extended $(\beta, \mathrm{St}/\mathrm{Fr})$ range. $\mathcal{F}(a_p)$ decreases for both buoyant and heavy particles, and the curves asymptotically reach the limits suggested by eq. (5) & (6). The present findings showcase the first evidence of intermittency reduction even for small St particles in turbulence.

Our results show that acceleration statistics (variance, correlation, and intermittency) is very sensitive to the ratio St/Fr. To explain the origin of these in physical terms, we consider the case of a particle drifting through a turbulent flow. As the particle drifts through the flow, it meets different eddies. Owing to its short response time, the particle readjusts to the velocity of these eddies. The rate at which the particle readjusts to the new eddies is linked to the spatial velocity gradients of the turbulent flow. As a consequence, the particle experiences accelerations that the regular fluid element does not experience,

thereby increasing its fluctuations (variance). The effect becomes prominent when the drifting time of the particle past the most energetic eddies (Taylor micro-scale eddies) becomes shorter than the timescale of these eddies of the flow, or when $\mathrm{St}/\mathrm{Fr} > 1$. This explains the scaling of the decorrelation time in Fig. 4(b) (see supplemental material [39] for details).

The same physical mechanisms could explain the decline in intermittency of particle acceleration. A drifting particle, instead of probing the accelerations of fluid elements, begins to sample the spatial gradients of the flow. An interesting analogy may be drawn to the intermittency of acceleration recorded by a hot-wire probe placed in a high-speed wind/water tunnel flow, where the probe effectively registers only the spatial gradients [47]. For a turbulent flow, the intermittency of the spatial gradients of velocity is lower as compared to the intermittency of the fluid element acceleration [3, 48]. Hence the observed decline in intermittency, which asymptotically approaches the expressions given by eq. (5) and (6) in the limit of large St/Fr. This gravity effect will be important even for moderate Stokes number particles, and the same qualitative trends may be expected. However, a moderate St particle responds slower to the turbulent eddies it drifts through. Hence, we expect the gravity effect to be less prominent than that for the $\mathrm{St} \ll 1$ particles we presented here, and this will be the focus of a future investigation.

In summary, the acceleration statistics of small Stokes number particles in turbulence is greatly modified in the presence of gravity. We report three major effects: an increase in acceleration variance, a decrease in correlation time, and a reduction of intermittency for buoyant and heavy particles. The ratio St/Fr governs the extent of this modification, as confirmed by our experiments using tiny air bubbles in water. Our theoretical predictions have broad validity – to particles of arbitrary density and even at large Reynolds numbers. Thus, a tiny bubble or droplet is not necessarily a good tracer of turbulent acceleration. This can be important for bubbles and droplets that drift through the turbulent oceans ($g/a_\eta \approx 100 - 1000$) and clouds ($g/a_\eta \approx 10 - 100$) [49]. On the practical side, our findings point to an important consideration when choosing bubbles or droplets for flow visualization and particle tracking in turbulent flows [21].

We gratefully acknowledge A. Prosperetti, S. S. Ray, G. D. Jin, S. Wildeman, and S. Maheshwari for insightful discussions. We thank S. Huisman, X. Zhu, P. Shukla and V. N. Prakash for comments which helped improve our manuscript. We thank the two anonymous referees for comments which helped improve our manuscript.

* enrico.calzavarini@polytech-lille.fr

† chaosun@tsinghua.edu.cn

[1] K. D. Squires and J. K. Eaton, Phys. Fluids A **3**, 1169 (1991).
[2] J. K. Eaton and J. Fessler, Int. J. Mult. Flow **20**, 169 (1994).
[3] F. Toschi and E. Bodenschatz, Annu. Rev. Fluid Mech. **41**, 375 (2009).
[4] M. Bourgoin and H. Xu, New J. Phys. **16**, 085010 (2014).
[5] A. Wood, W. Hwang, and J. Eaton, Int. J. Mult. Flow **31**, 1220 (2005).
[6] J. M. Mercado, D. C. Gomez, D. Van Gils, C. Sun, and D. Lohse, J. Fluid Mech. **650**, 287 (2010).
[7] R. Volk, E. Calzavarini, G. Verhille, D. Lohse, N. Mordant, J.-F. Pinton, and F. Toschi, Physica D: Nonlinear Phenomena **237**, 2084 (2008).
[8] L. Fiabane, R. Zimmermann, R. Volk, J.-F. Pinton, and M. Bourgoin, Phys. Rev. E **86**, 035301 (2012).
[9] E. Calzavarini, M. Cencini, D. Lohse, and F. Toschi, Phys. Rev. Lett. **101**, 084504 (2008).
[10] D. Lohse, Physics **1**, 18 (2008).
[11] T. Tanaka and J. K. Eaton, Phys. Rev. Lett. **101**, 114502 (2008).
[12] V. N. Prakash, Y. Tagawa, E. Calzavarini, J. M. Mercado, F. Toschi, D. Lohse, and C. Sun, New J. Phys. **14**, 105017 (2012).
[13] M. Cencini, J. Bec, L. Biferale, G. Boffetta, A. Celani, A. Lanotte, S. Musacchio, and F. Toschi, J. Turbulence p. N36 (2006).
[14] J. P. Salazar and L. R. Collins, Phys. Fluids **24**, 083302 (2012).
[15] E. Calzavarini, R. Volk, M. Bourgoin, E. Leveque, J. F. Pinton, and F. Toschi, J. Fluid Mech. **630**, 179 (2009).
[16] E. Calzavarini, M. Kerscher, D. Lohse, and F. Toschi, J. Fluid Mech. **607**, 13 (2008).
[17] H. Parishani, O. Ayala, B. Rosa, L.-P. Wang, and W. Grabowski, Phys. Fluids **27**, 033304 (2015).
[18] P. J. Ireland, A. D. Bragg, and L. R. Collins, arXiv preprint arXiv:1507.07022 (2015).
[19] J. Jung, K. Yeo, and C. Lee, Phys. Rev. E **77**, 016307 (2008).
[20] J. Bec, L. Biferale, G. Boffetta, A. Celani, M. Cencini, A. Lanotte, S. Musacchio, and F. Toschi, J. Fluid Mech. **550**, 349 (2006).
[21] S. Douady, Y. Couder, and M. Brachet, Phys. Rev. Lett. **67**, 983 (1991).
[22] C. R. Smith and R. D. Paxson, Exp. Fluids **1**, 43 (1983).
[23] L. J. Lu and C. R. Smith, Exp. Fluids **3**, 349 (1985).
[24] M. Holzner, A. Liberzon, N. Nikitin, B. Lüthi, W. Kinzelbach, and A. Tsinober, J. Fluid Mech. **598**, 465 (2008).
[25] J. M. Mercado, V. N. Prakash, Y. Tagawa, C. Sun, and D. Lohse, Phys. Fluids **24**, 055106 (2012).
[26] I. M. Mazzitelli and D. Lohse, New J. Phys. **6**, 203 (2004).
[27] G. Falkovich, A. Fouxon, and M. Stepanov, Nature **419**, 151 (2002).
[28] P. Falkowski, Nature **483**, S17 (2012).
[29] M. Maxey and S. Corrsin, J. Atm. Sci. **43**, 1112 (1986).
[30] M. Maxey, J. Fluid Mech. **174**, 441 (1987).
[31] M. Maxey, Phys. Fluids **30**, 1915 (1987).
[32] M. Maxey, Phil. Trans. Royal Soc. London **333**, 289 (1990).
[33] K. Gustavsson, S. Vajedi, and B. Mehlig, Phys. Rev. Lett. **112**, 214501 (2014).
[34] J. Bec, H. Homann, and S. S. Ray, Phys. Rev. Lett. **112**, 184501 (2014).

[35] G. Good, P. Ireland, G. Bewley, E. Bodenschatz, L. Collins, and Z. Warhaft, J. Fluid Mech. **759**, R3 (2014).
[36] K. Chang, B. J. Malec, and R. A. Shaw, New J Phys. **17**, 033010 (2015).
[37] R. Ni, S.-D. Huang, and K.-Q. Xia, J. Fluid Mech. **692**, 395 (2012).
[38] V. Mathai, V. N. Prakash, J. Brons, C. Sun, and D. Lohse, Phys. Rev. Lett. **115**, 124501 (2015).
[39] supplemental material available at URL. (2016).
[40] S. Ayyalasomayajula, A. Gylfason, L. R. Collins, E. Bodenschatz, and Z. Warhaft, Phys. Rev. Lett. **97**, 144507 (2006).
[41] R. D. Brown, Z. Warhaft, and G. A. Voth, Phys. Rev. Lett. **103**, 194501 (2009).
[42] V. Mathai, M. W. Neut, E. P. van der Poel, and C. Sun, Exp. Fluids **57**, 1 (2016).
[43] A. La Porta, G. A. Voth, A. M. Crawford, J. Alexander, and E. Bodenschatz, Nature **409**, 1017 (2001).
[44] R. Poorte and A. Biesheuvel, J. Fluid Mech. **461**, 127 (2002).
[45] E. Calzavarini, R. Volk, E. Leveque, J. F. Pinton, and F. Toschi, Physica (Amsterdam) **241D**, 237 (2012).
[46] T. Ishihara, Y. Kaneda, M. Yokokawa, K. Itakura, and A. Uno, J. Fluid Mech. **592**, 335 (2007).
[47] V. Sandborn, AIAA Journal **14**, 400 (1976).
[48] T. Ishihara, T. Gotoh, and Y. Kaneda, Annu. Rev. Fluid Mech. **41**, 165 (2009).
[49] B. Devenish, P. Bartello, J.-L. Brenguier, L. Collins, W. Grabowski, R. IJzermans, S. Malinowski, M. Reeks, J. Vassilicos, L.-P. Wang, et al., Quart. J. Royal Met. Soc. **138**, 1401 (2012).

arXiv:1606.02050v1 [physics.flu-dyn] 7 Jun 2016

Micro-bubbles and Micro-particles are Not Faithful Tracers of Turbulent Acceleration (Supplementary material)

Varghese Mathai,[1] Enrico Calzavarini,[2,*] Jon Brons,[1,3] Chao Sun,[4,1,†] and Detlef Lohse[1,5]

[1] *Physics of Fluids Group, Faculty of Science and Technology, Mesa+ Institute, University of Twente, 7500 AE Enschede, The Netherlands.*
[2] *Univ. Lille, CNRS, FRE 3723, LML, Laboratoire de Mecanique de Lille, F 59000 Lille, France*
[3] *Department of Mathematics and Physics, Faculty of Engineering and Computing, Coventry University, United Kingdom*
[4] *Center for Combustion Energy and Department of Thermal Engineering, Tsinghua University, 100084 Beijing, China.*
[5] *Max Planck Institute for Dynamics and Self-Organization, 37077 Göttingen, Germany.*

(Dated: August 22, 2016)

EXPERIMENTAL SETUP

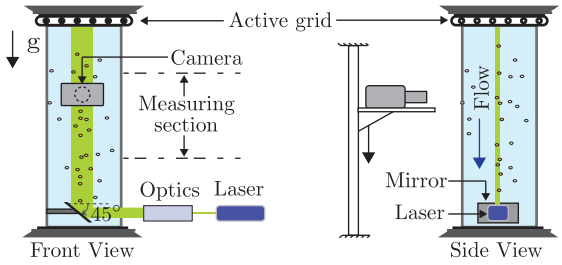

FIG. 1: Schematic of the measurement section of the Twente Water Tunnel. Bubbles and neutrally buoyant tracer particles of diameters $\approx$ 150 $\pm$ 25 μm and $\approx$ 125 μm, respectively, were dispersed in the flow for particle tracking experiments.

PARTICLE EQUATION OF MOTION

The model equation of motion for a small inertial spherical particle advected by a fluid flow field, with velocity $\mathbf{U}(\mathbf{X}(\mathcal{T}),\mathcal{T})$, is:

$$\mathcal{V}\,\rho_p\,\ddot{\mathbf{X}} = \mathcal{V}\,\rho_f\frac{D\mathbf{U}}{D\mathcal{T}} + \mathbf{F_{AM}} + \mathbf{F_D} + \mathbf{F_B} \qquad (1)$$

where $\mathcal{V} = \frac{4}{3}\pi a^3$ is the particle volume, with a being the particle radius, and ρ_f and ρ_p the fluid and particle mass densities, respectively. The forces contributing on the right-hand-side besides the fluid acceleration (which includes the pressure gradient term) are the added mass $\mathbf{F_{AM}}$, the drag force $\mathbf{F_D}$, and the buoyancy $\mathbf{F_B}$ [1–3]:

$$\mathbf{F_{AM}} = \mathcal{V}\,\rho_f C_M\left(\frac{D\mathbf{U}}{D\mathcal{T}} - \ddot{\mathbf{X}}\right), \qquad (2)$$

$$\mathbf{F_D} = 6\,\pi\,\mu\,a\,(\mathbf{U}-\dot{\mathbf{X}}), \qquad (3)$$

$$\mathbf{F_B} = \mathcal{V}\,(\rho_p-\rho_f)\,g\,\hat{\mathbf{e}}_z, \qquad (4)$$

where μ is the dynamic viscosity, g is the gravity intensity and $\hat{\mathbf{e}}_z$ is the unit-vector in the direction of gravity. Note that we use the inviscid added mass coefficient for a sphere, i.e $C_M = 1/2$. This leads to

$$\ddot{\mathbf{X}} = \frac{3\rho_f}{\rho_f+2\rho_p}\left(\frac{D\mathbf{U}}{D\mathcal{T}} + \frac{12\nu}{d_p^2}(\mathbf{U}-\dot{\mathbf{X}}) + g\,\hat{\mathbf{e}}_z\right) - g\,\hat{\mathbf{e}}_z, \qquad (5)$$

where $\nu \equiv \mu/\rho_f$ is the kinematic viscosity, and d_p is the particle diameter. Here we neglect lift, history, and finite-size Faxén forces, since these are verified to be small in point-particle limit and when the particle size is smaller than the Kolmogorov length scale η of the flow [4–6].

FROUDE NUMBER EFFECT

We first consider the effect of changing the ratio of turbulent to gravitational acceleration, i.e a_η/g, which, according to [7], equals the Froude number. Gravity enhances the acceleration in both vertical and horizontal directions (Fig. 2). The vertical acceleration is consistently lower compared to the horizontal, in agreement with our experiments. This is accompanied by a decrease in correlation time (Fig. 3), as also evidenced by our experiments.

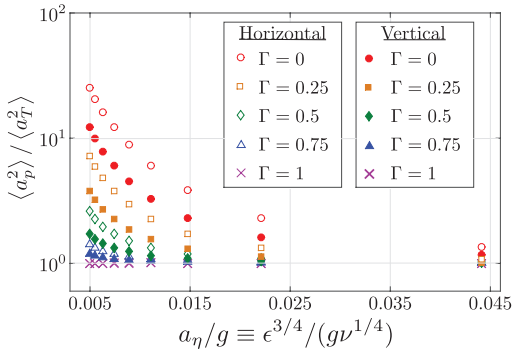

FIG. 2: Normalized acceleration variance for buoyant particles vs a_η/g obtained from Eulerian-Lagrangian DNS at $\mathrm{Re}_\lambda \approx 80$. Hollow and solid symbols correspond to horizontal and vertical components, respectively.

NON-DIMENSIONALIZATION

When the advecting flow is turbulent and the particle spatial extension is of the order of the dissipative scale of turbulence, it is appropriate to non-dimensionalize eq. (5) with respect to the Kolmogorov units: η (length) and τ_η (time). This leads to

$$\ddot{\mathbf{x}} = \beta\frac{D\mathbf{u}}{Dt} + \frac{1}{\mathrm{St}}(\mathbf{u} - \dot{\mathbf{x}}) + \frac{1}{\mathrm{Fr}}\hat{\mathbf{e}}_z, \tag{6}$$

where small case letters denote the new dimensionless variables and the following control parameters have been defined:

$$\beta \equiv \frac{3\rho_f}{\rho_f + 2\rho_p}; \quad \mathrm{St} \equiv \frac{d_p^2}{12\beta\nu\tau_\eta} = \frac{\tau_p}{\tau_\eta}; \quad \mathrm{Fr} \equiv \frac{a_\eta}{(\beta-1)\,g} \tag{7}$$

Note that the Stokes number St is defined taking added mass into account, and the Froude number Fr is a modified one that takes the particle density, through β, into account. Therefore these definitions are valid for a particle of arbitrary density.

In the high turbulence intensity limit ($\mathrm{Fr} \to \infty$), the third right-hand-side term in the equation of motion can be neglected. Under this condition the vanishing St limit leads to $\dot{\mathbf{x}} \simeq \mathbf{u}$ for the velocity, and for the acceleration to $\ddot{\mathbf{x}} \simeq D_t\mathbf{u}$, where $D_t\mathbf{u}$ denotes the fluid-tracer acceleration.

At finite Fr, the small St limit leads to $\dot{\mathbf{x}} \simeq \mathbf{u} + \frac{\mathrm{St}}{\mathrm{Fr}}\hat{\mathbf{e}}_z$. For the particle acceleration this implies:

$$\ddot{\mathbf{x}} \simeq D_t\mathbf{u} + \frac{\mathrm{St}}{\mathrm{Fr}}\partial_z\mathbf{u} \tag{8}$$

ACCELERATION VARIANCE

We consider the single-component acceleration variance. These are

$$\langle\ddot{x}^2\rangle \;\simeq\; \langle(D_t u_x)^2\rangle + \left(\frac{\mathrm{St}}{\mathrm{Fr}}\right)^2\langle(\partial_z u_x)^2\rangle, \tag{9}$$

$$\tag{10}$$

where x and z are the horizontal and vertical components, respectively. Note that the linear terms in St/Fr vanish because there is no correlation between terms of the type $\mathbf{u}\cdot\nabla u_i$ and $\partial_z u_i$, i.e. there is no instantaneous correlation between the velocity field and its gradient.

Under isotropic turbulent conditions, the following relations are verified [8]:

$$\langle(\partial_Z U_X)^2\rangle \simeq \frac{2}{15}\frac{\epsilon}{\nu}, \tag{11}$$

$$\langle(\partial_Z U_Z)^2\rangle \simeq \frac{1}{15}\frac{\epsilon}{\nu}, \tag{12}$$

$$\langle(D_\mathcal{T} U_i)^2\rangle = a_0\epsilon^{3/2}\nu^{-1/2}, \tag{13}$$

where i denotes one of the components x, y, or z, and a_0 is the so-called Heisenberg-Yaglom constant. From this, one obtains the relations linking the acceleration variance of particles to that of fluid tracers

$$\frac{\langle\ddot{x}^2\rangle}{\langle(D_t u_x)^2\rangle} \;\simeq\; 1 + \frac{2}{15a_0}\left(\frac{\mathrm{St}}{\mathrm{Fr}}\right)^2 \tag{14}$$

$$\frac{\langle\ddot{z}^2\rangle}{\langle(D_t u_x)^2\rangle} \;\simeq\; 1 + \frac{1}{15a_0}\left(\frac{\mathrm{St}}{\mathrm{Fr}}\right)^2 \tag{15}$$

These predictions are applicable to both heavy ($\mathrm{St/Fr} < 1$) and light ($\mathrm{St/Fr} > 1$) particles of arbitrary density. On the experimental side, we have confirmed the enhancement of acceleration variance using tiny air-bubbles dispersed in our water tunnel facility. For heavy-particles, our predictions remain to be experimentally verified.

LAGRANGIAN TIME CORRELATION

In Fig. 3(a), we plot the simulation results for the evolution of Lagrangian time-correlation of acceleration with the ratio St/Fr. The left branch points to heavy particle, and the right one, to light particles. With increasing magnitude of St/Fr, we observe a decline in the correlation time for both heavy and light particles. Clearly, the drifting of the buoyant or heavy particle through the flow affects the correlation time. We model this by considering the case of a particle drifting through the flow at a speed u_r. In the absence of particle drift, it is well-known that the decorrelation time is $\tau_T \sim \tau_\eta$ [9]. Based on the characteristic velocity of a particle in the turbulent flow, u_{rms}, we estimate the length scale corresponding to this decorrelation time as $\Lambda \sim u_{rms}\tau_\eta$. Now, for a buoyant or heavy particle, the time of correlation is reduced due to an extra drift speed. Therefore, the new correlation time may be written as $\tau_p \approx \tau_T/(1 + u_r/u_{rms})$. For homogeneous isotropic turbulence the u_{rms} may be expressed in terms of the Re_λ and the u_η. This leaves us with the expression: $\tau_p/\tau_\eta \approx 1/(1 + \sqrt[4]{5/(3\mathrm{Re}_\lambda^2)}\frac{\mathrm{St}}{\mathrm{Fr}})$. The predictions, shown by the solid black curve, are in reasonable agreement with our numerical observations.

While the model provides reasonable predictions for the decorrelation time, we observe some small deviations from small to moderate St/Fr values in Fig. 3(a). Below, we provide an explanation for these deviations. From eq. (8), we note that the acceleration of a drifting particle has two contributions: (a) $D_t\mathbf{u}$ from the fluid tracer acceleration, and (b) $\frac{\mathrm{St}}{\mathrm{Fr}}\partial_z\mathbf{u}$ from the velocity-gradients in the flow. In Fig. 3(b)-(e), we show the normalized time correlation of the particle accelerations and the gradient terms along the particle trajectories. For small St/Fr, the velocity gradient terms ($\partial_z u_z$ and $\partial_z u_x$) decorrelate slower as compared to the fluid acceleration term (see

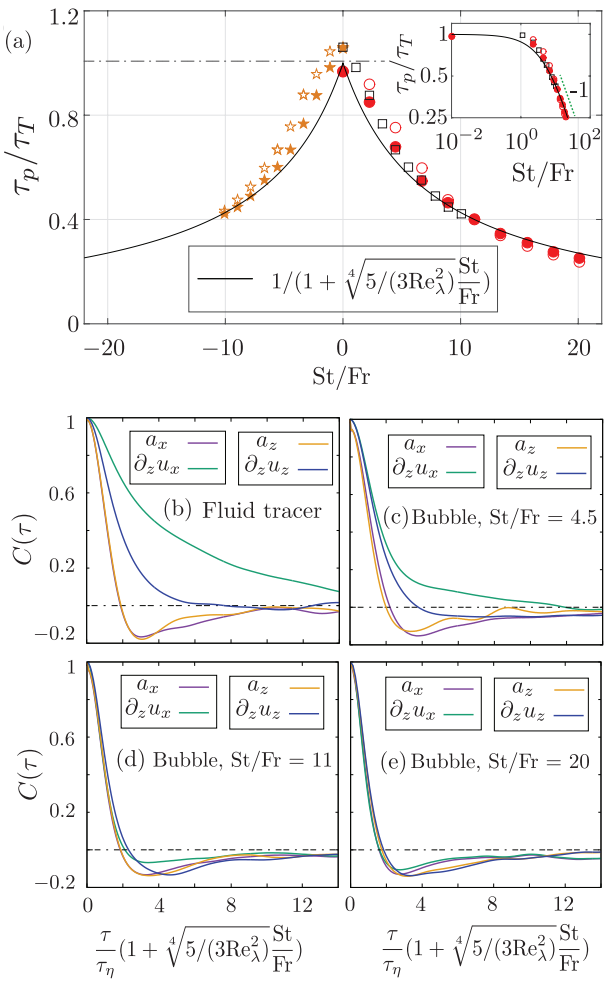

FIG. 3: (a) Normalized correlation time for bubbles ($\beta = 3$) and very heavy ($\beta = 0$) particles vs St/Fr obtained from Eulerian-Lagrangian DNS at $\mathrm{Re}_\lambda \approx 75$. The curve in black color shows the theoretical prediction, and the inset shows the plot on log-log scale. (b)-(e) Normalized autocorrelation function for fluid tracers and bubbles at different St/Fr values. Here, a_x and a_z are the horizontal and vertical accelerations, respectively. $\partial_z u_x$ and $\partial_z u_z$ are the spatial-velocitiy gradients, which contribute to the a_x and a_z, respectively. In (c)-(e) St/Fr increases from 4.5 to 20.

Fig. 3(b) & (c)). Since St/Fr is small, the fluid acceleration term $D_t\mathbf{u}$ dominates over the velocity gradient term $\frac{\mathrm{St}}{\mathrm{Fr}}\partial_z\mathbf{u}$. This explains the slower decrease in the decorrelation time in the numerics as compared to our predictions for small St/Fr (see |St/Fr|< 5 in Fig. 3(a)). Some additional observations may be made for the moderate St/Fr range. From Fig. 3(a), we note that the vertical component of particle acceleration (solid symbols) is shorter-correlated compared to the horizontal component (hollow symbols). This occurs because the fluid velocity gradient components are not all correlated in the same way. Due to the incompressibility constraint ($\partial_i u_i = 0$), the longitudinal gradient $\partial_z u_z$ is shorter-correlated compared to the transverse gradient $\partial_z u_x$, as may be seen in Fig. 3(b) & (c). Since the vertical acceleration is influenced by the longitudinal velocity-gradient, it decorrelates in shorter time than the horizontal acceleration. We now consider the case of large St/Fr in Fig. 3(a). In this case, the velocity gradient term $\frac{\mathrm{St}}{\mathrm{Fr}}\partial_z\mathbf{u}$ in eq. (8) dominates over the fluid acceleration term $D_t\mathbf{u}$, and therefore, the decrease in correlation time in DNS is in good agreement with the predictions of our eddy-crossing model.

ACCELERATION INTERMITTENCY

Intermittency, i.e. the observed strong deviations from Gaussianity, can be characterized in terms of the flatness of acceleration $\mathcal{F}(a_p) \equiv \langle a_p^4 \rangle / \langle a_p^2 \rangle^2$. Assuming statistical independence between $D_t u_i$ and $\partial_z u_i$[1], we obtain the tracer-normalized flatness of particle acceleration,

$$\frac{\mathcal{F}(\ddot{x})}{\mathcal{F}(D_t u_x)} = \frac{1 + \frac{12}{15\ a_0 \mathcal{F}(D_t u_x)} \left(\frac{\mathrm{St}}{\mathrm{Fr}}\right)^2 \left(1 + \frac{\mathcal{F}(\partial_z u_x)}{45\ a_0} \left(\frac{\mathrm{St}}{\mathrm{Fr}}\right)^2\right)}{1 + 2\frac{2}{15\ a_0}\left(\frac{\mathrm{St}}{\mathrm{Fr}}\right)^2 + \left(\frac{2}{15\ a_0}\right)^2 \left(\frac{\mathrm{St}}{\mathrm{Fr}}\right)^4} \tag{16}$$

$$\frac{\mathcal{F}(\ddot{z})}{\mathcal{F}(D_t u_x)} = \frac{1 + \frac{6}{15\ a_0 \mathcal{F}(D_t u_x)} \left(\frac{\mathrm{St}}{\mathrm{Fr}}\right)^2 \left(1 + \frac{\mathcal{F}(\partial_z u_z)}{90\ a_0} \left(\frac{\mathrm{St}}{\mathrm{Fr}}\right)^2\right)}{1 + 2\frac{1}{15\ a_0}\left(\frac{\mathrm{St}}{\mathrm{Fr}}\right)^2 + \left(\frac{1}{15\ a_0}\right)^2 \left(\frac{\mathrm{St}}{\mathrm{Fr}}\right)^4} \tag{17}$$

In the limit of small St/Fr,

$$\frac{\mathcal{F}(\ddot{x})}{\mathcal{F}(D_t u_x)} \simeq 1 - \frac{4}{15\ a_0}\left(1 - \frac{3}{\mathcal{F}(D_t u_x)}\right)\left(\frac{\mathrm{St}}{\mathrm{Fr}}\right)^2 \tag{18}$$

$$\frac{\mathcal{F}(\ddot{z})}{\mathcal{F}(D_t u_x)} \simeq 1 - \frac{2}{15\ a_0}\left(1 - \frac{3}{\mathcal{F}(D_t u_x)}\right)\left(\frac{\mathrm{St}}{\mathrm{Fr}}\right)^2 \tag{19}$$

It is verified that $\mathcal{F}(D_t u_x) > 3$. Therefore, both components are decreasing functions of St/Fr, with the vertical being larger than the horizontal one for small St/Fr.
In the large St/Fr limit,

$$\frac{\mathcal{F}(\ddot{x})}{\mathcal{F}(D_t u_x)} \simeq \frac{\mathcal{F}(\partial_z u_x)}{\mathcal{F}(D_t u_x)} \tag{20}$$

$$\frac{\mathcal{F}(\ddot{z})}{\mathcal{F}(D_t u_x)} \simeq \frac{\mathcal{F}(\partial_z u_z)}{\mathcal{F}(D_t u_x)} \tag{21}$$

It is verified that $\mathcal{F}(\partial_z u_z) < \mathcal{F}(\partial_z u_x) < \mathcal{F}(D_t u_x)$ [10]. This leads to the prediction $\mathcal{F}(a_v) < \mathcal{F}(a_h)$ i.e. vertical acceleration is less intermittent compared to the horizontal.

INTERPRETATION

Eq. (18)-(19) and eq. (20)-(21) provide predictions for the normalized acceleration flatness (intermittency) in the limits

[1] The absence of correlations between $D_t u_i$ and $\partial_z u_i$ is a first order (to be refined) approximation.

of small St/Fr and large St/Fr, respectively. Eq. (18)-(19) predict that the vertical component of flatness exceeds the horizontal one in the small St/Fr limit, while eq. (20)-(21) predict that the horizontal component exceeds the vertical one when St/Fr is large. Therefore, an interesting cross-over is predicted between the flatness factors of the two components as one moves from small St/Fr to large St/Fr. In Fig. 4, we present our numerical results in the small St/Fr range (St/Fr < 1). Despite the scatter in data, we make some interesting observation about our numerical results. With the exception of a single datapoint, the vertical components (solid symbols) are always higher compared to the horizontal components (hollow symbols), in agreement with eq. (18)-(19). In the large St/Fr limit, as was clear from Figure 4(c) of the main paper, the horizontal component exceeded the vertical one, again in agreement with our predictions (eq. (20)-(21)). Therefore, the cross-over predicted by us is qualitatively seen in our simulations as well. A quantitative agreement is missing since the higher moments (Flatness) are in general very sensitive. Moreover, the lowest Stokes numbers possible in simulations is ≈ 0.05, which is still an approximation of the St $\to 0$ limit. In addition, the predictions are subject to a few assumptions, such as the absence of correlation between velocity field and its gradient. While this is reasonable, it is not an exact result. At present, we do not have the resolution to verify the intricate details of (18)-(19). These aspects may be tested in future studies.

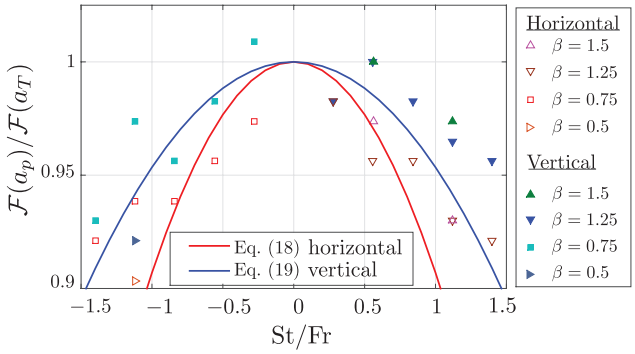

FIG. 4: Normalized Flatness factor in the small St/Fr limit. Hollow symbols show the flatness fo horizontal acceleration. Solid symbols show the flatness of vertical acceleration. The vertical acceleration flatness is mostly higher in numerics, in qualitative agreement with the predictions of eq. (18)-(19).

A GENERALIZED APPROACH

We discuss some of these recent analytical and numerical approaches for heavy particles. Interesting effects have been demonstrated on the gravity-induced modification of heavy particle statistics [7, 11–14], which were quantified as a function of particle inertia (St) and the Froude number given by the ratio of turbulent to gravitational acceleration (a_η/g). We examine the Stokes and Froude number definitions used in these studies. The Stokes number was defined as $\mathrm{St} \equiv \frac{\rho_p d_p^2}{18\rho_f \nu \tau_\eta}$ [7, 12, 14]. This definition is appropriate at large ρ_p/ρ_f, when added mass effects are negligible. We also note that the definition of Froude number as a_η/g [7, 14] does not take the particle density into account. Here, a_η is the turbulent acceleration and g is the gravitational acceleration. This Froude number definition is applicable when the particles under consideration are of fixed ρ_p/ρ_f. Therefore, these results apply to the case of very heavy particles and when the density ratio is kept constant, i.e $\rho_p/\rho_f = \text{constant} \gg 1$.

In this paper (main article), we provide a generalized description that is applicable to particles of arbitrary density. We have numerically shown the validity of our theoretical preditions for particles of arbitrary density. The theory we develop for isotropic turbulence can explain also our experimental findings on bubbles in a turbulent water flow. The generic St and Fr definitions we use converge to the definitions in [7, 12, 14] at large ρ_p/ρ_f. Therefore, such a modified approach may be useful for future studies that explore the effects of gravity for arbitrary-density particles in turbulence.

* enrico.calzavarini@polytech-lille.fr
† chaosun@tsinghua.edu.cn

[1] M. R. Maxey and J. J. Riley, Phys. Fluids **26**, 883 (1983).
[2] R. Gatignol, J. Mec. Theor. Appl. **2**, 143 (1983).
[3] P. Spelt and A. Biesheuvel, J. Fluid Mech. **336**, 221 (1997).
[4] E. Calzavarini, R. Volk, E. Leveque, J. F. Pinton, and F. Toschi, Physica (Amsterdam) **241D**, 237 (2012).
[5] E. Calzavarini, R. Volk, M. Bourgoin, E. Leveque, J. F. Pinton, and F. Toschi, J. Fluid Mech. **630**, 179 (2009).
[6] Y. Tagawa, J. M. Mercado, V. N. Prakash, E. Calzavarini, C. Sun, and D. Lohse, J. Fluid Mech. **693**, 201 (2012).
[7] J. Bec, H. Homann, and S. S. Ray, Phys. Rev. Lett. **112**, 184501 (2014).
[8] J. Hinze, *0. 1975 turbulence* (1972).
[9] P. Yeung and S. Pope, J. Fluid Mech. **207**, 531 (1989).
[10] T. Ishihara, Y. Kaneda, M. Yokokawa, K. Itakura, and A. Uno, J. Fluid Mech. **592**, 335 (2007).
[11] K. Gustavsson, S. Vajedi, and B. Mehlig, Phys. Rev. Lett. **112**, 214501 (2014).
[12] H. Parishani, O. Ayala, B. Rosa, L.-P. Wang, and W. Grabowski, Phys. Fluids **27**, 033304 (2015).
[13] A. Aliseda, A. Cartellier, F. Hainaux, and J. C. Lasheras, J. Fluid Mech. **468**, 77 (2002).
[14] P. J. Ireland, A. D. Bragg, and L. R. Collins, arXiv preprint arXiv:1507.07022 (2015).